Dalton Transactions

Accepted Manuscript

This is an *Accepted Manuscript*, which has been through the RSC Publishing peer review process and has been accepted for publication.

Accepted Manuscripts are published online shortly after acceptance, which is prior to technical editing, formatting and proof reading. This free service from RSC Publishing allows authors to make their results available to the community, in citable form, before publication of the edited article. This *Accepted Manuscript* will be replaced by the edited and formatted *Advance Article* as soon as this is available.

To cite this manuscript please use its permanent Digital Object Identifier (DOI®), which is identical for all formats of publication.

More information about *Accepted Manuscripts* can be found in the **Information for Authors**.

Please note that technical editing may introduce minor changes to the text and/or graphics contained in the manuscript submitted by the author(s) which may alter content, and that the standard **Terms & Conditions** and the **ethical guidelines** that apply to the journal are still applicable. In no event shall the RSC be held responsible for any errors or omissions in these *Accepted Manuscript* manuscripts or any consequences arising from the use of any information contained in them.

Dalton Transactions

Dalton Transactions

Dynamic Article Links ►

Cite this: DOI: 10.1039/c0xx00000x

www.rsc.org/materials

PAPER

Structural relationships among LiNaMg[PO_4]F and Na_2M[PO_4]F (M = Mn-Ni, and Mg), and the magnetic structure of LiNaNi[PO_4]F

Hamdi Ben Yahia[a,*], Masahiro Shikano[a,*], Hironori Kobayashi[a], Maxim Avdeev[b], Samuel Liu[c], Chris D. Ling[c]

Received (in XXX, XXX) Xth XXXXXXXXX 2011, Accepted Xth XXXXXXXXX 20XX
DOI: 10.1039/b000000x

The new compound LiNaMg[PO_4]F has been synthesized by wet chemical reaction route. Its crystal structure was determined from single-crystal X-ray diffraction data. LiNaMg[PO_4]F crystallizes with the monoclinic pseudomerohedrally twinned LiNaNi[PO_4]F structure, space group $P2_1/c$, a = 6.772(4), b = 11.154(6), c = 5.021(3) Å, β = 90.00(1) ° and Z = 4. The structure contains $[MgO_3F]_n$ chains made up of zigzag edge-sharing MgO_4F_2 octahedra. These chains are interlinked by PO_4 tetrahedra forming 2D-Mg[PO_4]F layers. The alkali metal atoms are well ordered in between these layers over two atomic positions. The use of group-subgroup transformation schemes in the Bärnighausen formalism enabled us to determine precise phase transition mechanisms from LiNaNi[PO_4]F- to Na_2M[PO_4]F-type structures (M = Mn-Ni, and Mg) (see video clip1 and 2). The crystal and magnetic structure and properties of the parent LiNaNi[PO_4]F phase were also studied by magnetometry and neutron powder diffraction. Despite rather long interlayer distance, $d_{min}(Ni^{+2}\text{-}Ni^{+2})$~6.8 Å, the material develops long-range magnetic order below 5 K. The magnetic structure can be viewed as antiferromagnetically coupled ferromagnetic layers with moments parallel to the b-axis.

1. Introduction

There have been a number of studies on compounds of the formula $AMPO_4$, where A is an alkali atom and M is a transition metal.[1and ref. therein] The crystal structures of $AMPO_4$ depend strongly on the size of the monovalent A^+ cation. With A = Li, the $AMPO_4$ compounds adopt the olivine-type structure. Since the study of its electrochemical properties by Goodenough et al.,[2] LiFePO_4 has been extensively studied among the olivine series LiMPO_4. Several studies have shown that LiFePO_4 is a promising high-potential cathode material for rechargeable Li-ion batteries.[3-5] With A = Na, the $AMPO_4$ (M = Mn-Co) compounds have the maricite-type structure.[6]

When the LiMPO_4 (M = Mg, Co, Ni) compounds are mixed with LiF, the Li_2MPO_4F fluorophosphates are formed and they crystallize with the 3D-Li_2NiPO_4F-type structure.[7-8] The Li_2MPO_4F (M = Mn, Fe) phases could not be synthesised using conventional synthesis routes. However, these phases could be obtained by electrochemical ion exchange starting from the Na_2MnPO_4F and by lithium intercalation into the tavorite LiFePO_4F.[9-11] When the NaMPO_4 (M = Mn-Ni and Mg) compounds are mixed with NaF, the Na_2MPO_4F fluorophosphates are formed and they crystallize with three different layered structures strongly related to each other.[12 and ref. therein]

Since, the crystal structures of the A_2MPO_4F compounds are very sensitive to any volume change, related to the size of the alkali metal or the transition metal atoms, our research group has recently focused on the synthesis and the study of the physical properties of new compositions. Indeed, we succeeded to discover several phases (LiNaCo[PO_4]F, $Li_{2-x}Na_xFe$[PO_4]F, $LiNaFe_{1-x}Mn_x$[PO_4]F, and Li_2Mg[PO_4]F crystallizing with the Li_2Ni[PO_4]F-type structure and LiNaMg[PO_4]F, LiNaNi[PO_4]F, and Na_2Ni[PO_4]F crystallizing with two different layered structures).[12-16] Furthermore, we discovered $Li_9Mg_3[PO_4]_4F_3$ which crystallizes with a new structure type closely related to Na_2Mn[PO_4]F and which exhibits a high ionic conductivity σ of 10^{-4} S cm^{-1} at 300 °C.[17]

In this paper, we report the crystal structure study of the new compound LiNaMg[PO_4]F and discuss in details its structural relationship to the Na_2M[PO_4]F (M = Mn-Ni, and Mg) compounds. We also characterized the parent LiNaNi[PO_4]F phase by powder neutron diffraction and magnetic susceptibility measurements. This work is a complement to the previously studied $Li_{2-x}Na_xNi$[PO_4]F system.

*,[a]*Research Institute for Ubiquitous Energy Devices, National Institute of Advanced Industrial Science and Technology (AIST), Midorigaoka 1-8-31, Ikeda, Osaka 563-8577, Japan. Fax: +81-72-751-9609; Tel: +81-72-751-7932;E-mail:benyahia.hamdi@voila.fr,shikano.masahiro@aist.go.jp.*
[b]Bragg Institute, B87, Australian Nuclear Science and Technology Organisation, Locked Bag 2001 Kirrawee DC NSW 2232, Australia.
[c] School of Chemistry, The University of Sydney, Sydney, NSW 2006, Australia.
† Electronic Supplementary Information (ESI) available: See DOI: 10.1039/b000000x/

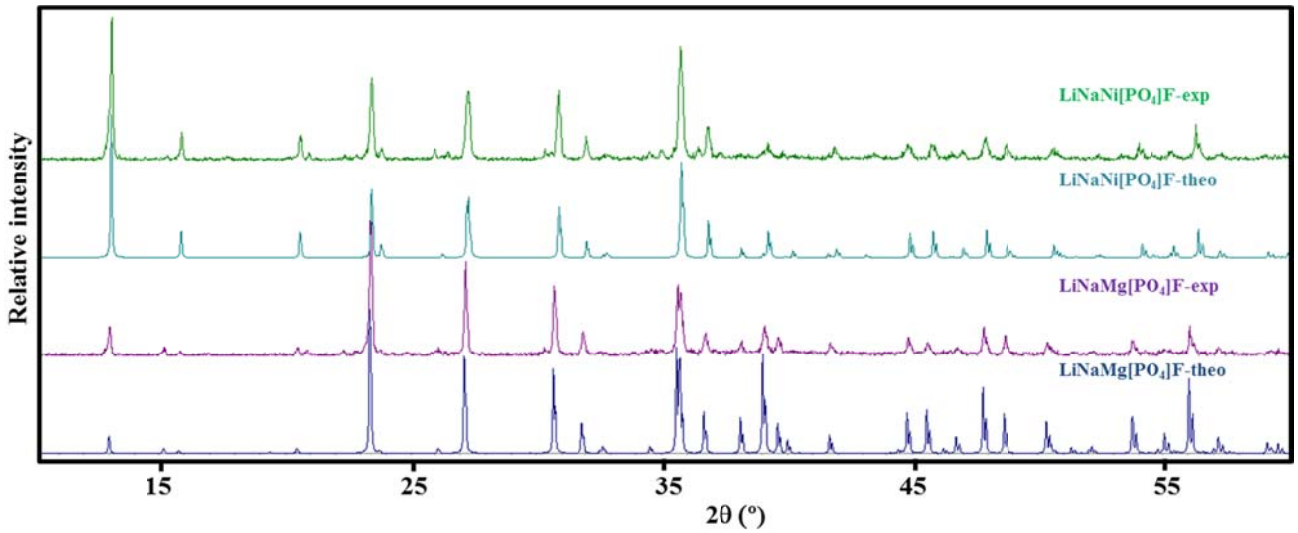

Fig. 1. Superposition of the theoretical and experimental powder XRD (Cu-$K\alpha_{1},\alpha_{2}$ radiation) patterns of $LiNaMg[PO_4]F$ and $LiNaNi[PO_4]F$ samples.

2. Experimental Section

2.1. Synthesis

A polycrystalline (powder) samples of $LiNaMg[PO_4]F$ and $LiNaNi[PO_4]F$ were prepared by direct solid-state reaction from stoichiometric mixture of NaF, $LiMg[PO_4]$ ($LiMg[PO_4]$ was obtained by heating a 1:2:2 mixture of Li_2CO_3, MgO, and $(NH_4)H_2PO_4$ at 350 °C for 6 h and at 750 °C for 24 h) and $LiNi[PO_4]$ (Fig. 1) ($LiNi[PO_4]$ was obtained by heating a 1:2:2 mixture of Li_2CO_3, NiO, and $(NH_4)H_2PO_4$ at 350 °C for 6 h, at 700 °C for 10 h and at 850 °C for 18 h). The mixtures were wet-ball milled in ethanol for 2 h in a planetary ball-mill. The mixed slurries were dried, pelletized and fired at 580 °C for 48h. $LiNaMg[PO_4]F$ was also prepared by a wet chemical route from a stoichiometric mixture of LiF, $NaNO_3$, $NH_4H_2PO_4$, and $Mg(NO_3)_2{\cdot}6H_2O$. The starting materials were dissolved in boiling deionized water then left stirring for a few hours until the water had evaporated. The obtained powder was then pelletized and heated at 600 °C for 8 h in a platinum crucible under air. This produced $LiNaMg[PO_4]F$ as a major phase alongside a tiny amount of non-identified impurities. This mixture was placed in a platinum tube and fired at 1000 °C, then slowly cooled to room temperature at a rate of 15 °C/h. After washing the mixture with distilled water, colorless single crystals of $LiNaMg[PO_4]F$ and $LiMg[PO_4]$ were identified in the sample using a combination of energy-dispersive X-ray (EDX) and single crystal X-ray diffraction (XRD) analyses.

2.2. Electron microprobe analysis

Semiquantitative EDX analyses of different single crystals including the ones investigated on the diffractometer were carried out with a Genesis (EDAX) analyzer installed a JSM-500LV (JEOL) scanning electron microscope (SEM). The experimentally observed compositions of the carbon coated material were close to the ideal $LiNaMg[PO_4]F$ (Fig. 2). The resolution of the instrument was not sufficient to determine the lithium content.

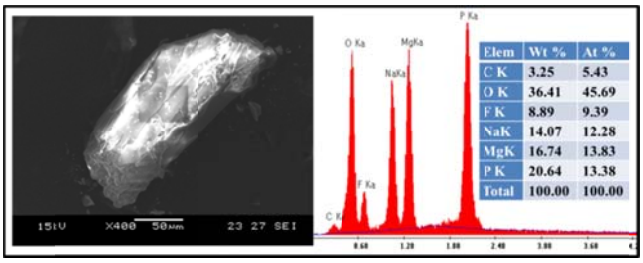

Fig. 2. SEM image and EDX analysis of the $LiNaMg[PO_4]F$ single crystal used for data collection.

2.3. X-Ray diffraction

To check the purity of the $LiNaMg[PO_4]F$ powder, routine powder XRD measurements were performed. Data were collected at room temperature over the 2θ angle range $10\ ° \leq 2\theta \leq 80\ °$ with a step size of 0.01 ° using a RINT2000-TTR (Rigaku) diffractometer operating with Cu$K\alpha_{1},\alpha_{2}$ radiation. Full pattern-matching refinement was performed with the Jana2006 program.[18] The background was modelled using a Legendre function, and the peak shape by a pseudo-Voigt function (Fig. S1).† The refined unit cell parameters were a = 6.8144(4), b = 11.1974(7), c = 5.0155(3) Å, β = 90.00(1) ° and V = 382.70(6) $Å^3$, in good agreement with the single crystal data presented in Table S1.

Single crystals of $LiNaMg[PO_4]F$ suitable for XRD were selected on the basis of the size and the sharpness of the diffraction spots. Data collection was carried out on a SMART APEX (Bruker) diffractometer using Mo$K\alpha$ radiation. Data processing and all refinements were performed with the Jana2006 program. A Gaussian-type absorption correction was applied and the shape was determined with the video microscope. For data collection details, see Table S1.

2.4. Magnetic susceptibility measurements

Magnetic susceptibility measurements of $LiNaNi[PO_4]F$ were carried out using a Quantum Design Physical Properties Measurement System (PPMS) with a vibrating sample magnetometer (VSM) probe. The susceptibility was recorded in

the zero field-cooled mode over the temperature range 2–300 K under the field of 100 Oe.

2.5. Neutron powder diffraction

Neutron powder diffraction (NPD) data were collected on the high-resolution diffractometer Echidna at the OPAL facility (Lucas Heights, Australia) using neutrons of wavelength 2.4395 Å. For the measurements, ~2 g of the powder sample was loaded into a 6 mm diameter cylindrical vanadium can and data collected between 3 and 6 K, i.e., above and below the magnetic transition, using a closed-cycle refrigerator. Rietveld analysis of the data was performed using the Fullprof Suite with the default neutron scattering lengths and Ni^{2+} magnetic form-factor.

3. RESULTS AND DISCUSSION

3.1. Structure refinement

The cell parameters determined for $LiNaMg[PO_4]F$ suggest orthorhombic symmetry; however, the apparent systematic absences were not consistent with any known orthorhombic space group. Therefore, we first solved the structure in the triclinic space group $P\bar{1}$. Most of the atomic positions were located using the sir2004 program.[19] After few refinement cycles followed by difference-Fourier syntheses, the whole structure was determined (18 atoms). Then, using the Platon suite of crystallographic programs,[20] we determined that a higher symmetry exists with a monoclinic space group $P2_1/c$. Starting from the triclinic structural model and changing the space group from $P\bar{1}$ to $P2_1/c$ reduced the number of independent atomic positions by a factor of two. Using isotropic atomic displacement parameters (ADP), the residual factors converged to $R(F) = 0.2617$ and $wR(F^2) = 0.532$ for 37 refined parameters. With anisotropic ADPs, the residual factors did not decrease, $R(F) = 0.2473$ and $wR(F^2) = 0.5116$ for 82 refined parameters. The refinement of the alkali metal occupancies did not show any significant deviation from the expected values. At this stage of the refinement, all the atoms were well-behaved, although the high values of the reliability factors and the goodness-of-fit ($s = 7.6$) clearly hinted at a symmetry problem, most likely twinning. Therefore, the Platon suite program was used to test possible twinning of the structure. The two-fold axis parallel to c was identified as a possible twinning element, and on this basis we introduced the twin matrix (-1 0 0, 0 -1 0, 0 0 1). By incorporating this twinning option, the residuals immediately dropped drastically to the values listed in Table S1. There are three other possible twin matrixes (a consequence of the coset decomposition) which can be used and which lead to the same refinement result; $2_{[100]}$, $m_{[100]}$, and $m_{[001]}$. Inspection of databases revealed a structural relationship to $LiNaNi[PO_4]F$.[12] The refined atomic positions and anisotropic ADP are given in Tables 1 and S2,† respectively. Further details on the structure refinements may be obtained from the Fachinformationszentrum Karlsruhe, D-76344 Eggenstein-Leopoldshafen, by quoting the Registry No. CSD-426199.

Crystallographers and others will note that we used a monoclinic space group $P2_1/c$ with the $\beta = 90$ ° which is extremely rare and usually indicates higher symmetry. Therefore, we have attempted to confirm the symmetry by closely examining the structure. Indeed, in theoretical point of view, it is possible to use the *Pnma* space group to solve the structure, however in this case a Na/Mg statistical disorder is observed at the 8*d* atomic position. Therefore, in order to obtain a perfectly ordered structure it is necessary to decrease the symmetry from *Pnma* to $P2_1/c$. This induces the splitting of the 8*d* atomic position into 2 × 4*e* ($P2_1/c$) atomic positions, in which are located the ordered Mg and Na atoms (For more details see section 3.4. of ref. 12).

Table 1. Atom positions and isotopic ADPs (Å^2) for $LiNaMg[PO_4]F$.

Atom	*x*	*y*	*z*	U_{eq} (Å^2)
Li	0.7408(5)	0.9196(3)	0.7635(7)	0.0068(12)
Na	0.51155(15)	0.83455(9)	0.2530(2)	0.0199(4)
Mg	0.01886(12)	0.17115(7)	0.76322(16)	0.0082(2)
P	0.75454(9)	0.08170(5)	0.27092(12)	0.00751(19)
O1	0.5429(2)	0.12366(16)	0.2405(3)	0.0143(5)
O2	0.8905(3)	0.17177(16)	0.1317(4)	0.0143(5)
O3	0.8051(3)	0.07394(15)	0.5700(4)	0.0126(5)
O4	0.7828(3)	0.95910(14)	0.1428(3)	0.0119(5)
F	0.1990(2)	0.28708(13)	0.9647(3)	0.0137(4)

3.2. Crystal structure

$LiNaMg[PO_4]F$ was thereby found to be isostructural with $LiNaNi[PO_4]F$, which crystallizes with a layered structure.[12] It is a monoclinic pseudomerohedrally twinned structure consisting of $Mg[PO_4]F$ layers with lithium and sodium atoms well-ordered in the interlayer space (Fig. 3a). Magnesium atoms are octahedrally coordinated to four oxygen and two fluorine atoms. These octahedra share edges (*via* 1F and 1O) and form infinite chains running along the *c* axis. These chains are connected by PO_4 tetrahedra to form $Mg[PO_4]F$ layers (Fig. 3b) between which lie lithium and sodium atoms. The interatomic distances Na-*X*, Mg-*X*, and P-O are listed in Table 2.

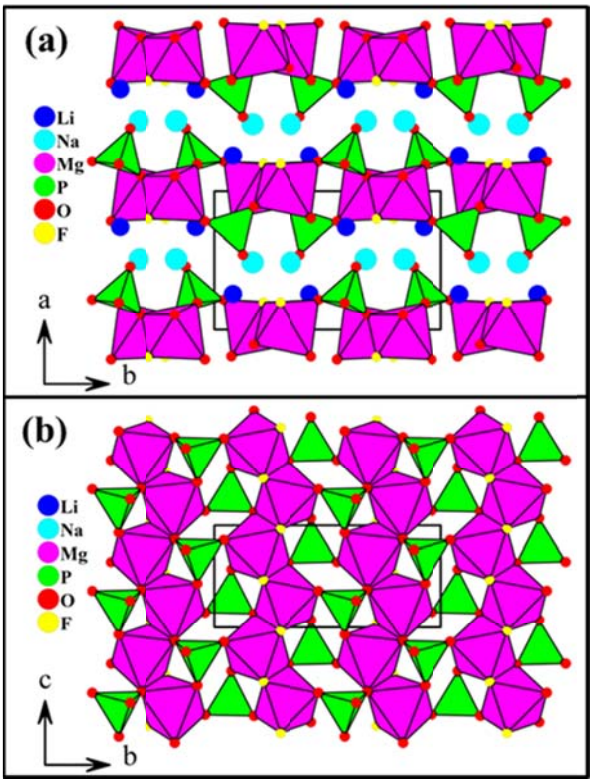

Fig. 3. Projection view of the structure of $LiNaMg[PO_4]F$ in the (001) plane (a) and projection view of the $Mg[PO_4]F$ layer on the (100) plane (b).

Table 2. Interatomic distances (in Å) and bond valence sums (BVS) for LiNaMg[PO_4]F. Average distances are given in brackets.

	distance	BV		distance	BV
Li-F	1.922(4)	0.219	Na-O4	2.384(2)	0.208
Li-O1	1.994(4)	0.240	Na-O1	2.396(2)	0.201
Li-O4	1.977(4)	0.251	Na-F	2.4878(18)	0.112
Li-O3	2.034(4)	0.215	Na-O3	2.550(2)	0.133
Li-F	2.722(4)	0.025	Na-O1	2.550(2)	0.133
Li-O2	2.766(4)	0.030	Na-O1	2.613(2)	0.112
<Li-*X*>	1.982[4]	0.925[4] [a]	Na-F	2.6372(18)	0.075
Mg-F	1.9937(16)	0.390	<Na-*X*>	2.5168[7]	0.974[7] [a]
Mg-O4	2.0464(19)	0.385			
Mg-O2	2.047(2)	0.384	P-O1	1.5252(18)	1.282
Mg-F	2.0554(17)	0.330	P-O4	1.5313(17)	1.261
Mg-O3	2.063(2)	0.368	P-O2	1.5393(19)	1.234
Mg-O2	2.076(2)	0.355	P-O3	1.5438(19)	1.219
<Mg-*X*>	2.0469[6]	2.212[6] [a]	<P-O>	1.5349[4]	4.996[4] [a]

[a] bond valence sum, BV = $\exp\{(r_0-r)/b\}$ with the following parameters: b = 0.37, r_0 (Li^I–O) = 1.466, r_0 (Li^I–F) = 1.36, r_0 (Na^I–O) = 1.803, r_0 (Na^I–F) = 1.677, r_0 (Mg^{II}–O) = 1.693, r_0 (Mg^{II}–F) = 1.645 and r_0 (P^V–O) = 1.617 Å.[21, 22]

In LiNaMg[PO_4]F, the MgO_4F_2 octahedra are regular in shape with Mg-*X* distances ranging from 1.9937 to 2.076 Å and an average value of 2.0469 Å. No significant difference in Mg coordination is observed compared to $Li_2Mg[PO_4]F$ and $Na_2Mg[PO_4]F$, although the latter structures belong to a different structure types.[17, 23] The PO_4 tetrahedra are also quite regular, with P-O distances ranging from 1.5252 to 1.5438 Å with an average value of 1.5349 Å, only slightly lower than the value of 1.55 Å estimated from the effective ionic radii of the four-coordinated P^{5+} and O^{2-}.[24] The sodium atoms are coordinated to five oxygen and two fluorine atoms (Fig. 4a). The Na-*X* distances range from 2.384 and 2.6372 Å with an average value of 2.5168 Å. This sodium environment is similar to sodium polyhedra in LiNaNi[PO_4]F (Fig. 4b). The lithium atoms are four coordinated to three oxygen and one fluorine atoms (Fig. 4a). The Li-*X* distances range from 1.922 and 2.034 Å with an average value of 1.982 Å. The BVS of 0.925, 0.974, 2.212, and 4.996 are in very good agreement with the expected value of +1, +1, +2, and +5 for Li^+, Na^+, Mg^{2+}, and P^{5+}, respectively.

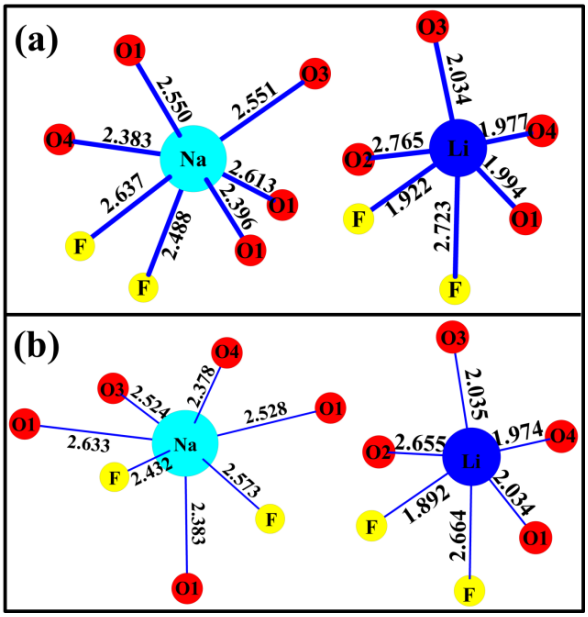

Fig. 4. Surrounding of the sodium and lithium atoms in LiNaMg[PO_4]F (a), and LiNaNi[PO_4]F (b).

3.3. Structural relationship of $A_2M[PO_4]F$ (*A* = Li and Na; *M* = Mn-Ni, and Mg) to other known oxides.

In the supplementary information section, we have demonstrated that each $Na_2M[PO_4]F$ unit cell is a supercell of an orthorhombic subcell, similar to LiNaNi[PO_4]F (Table S3).[25-44] Consequently, starting from an orthorhombic subcell (a_{o1} ~ 6.75 Å, b_{o1} ~ 5 Å, and c_{o1} ~ 11 Å) and using the geometric relationships given in Fig. 5q, it is possible to build an orthorhombic supercell (a_{o2} = ~ 13.5 Å, $b_{o2} = b_{o1}$ ~ 5 Å, and $c_{o2} = c_{o1}$ ~ 11 Å) (Fig. 5o) or a monoclinic supercell (a_m = ~ 13.5 Å, $b_m = b_{o1}$ ~ 5 Å, and c_m = ~ 12.9Å) (Fig. 5p) which are very similar to the $Na_2M[PO_4]F$ unit cells Fig. 5a-c.

A projection view of the fluorophosphates along the short axis (~5 Å) shows the layered character of the structures (Fig. 5a-e). In all cases, the structures are built of $M[PO_4]F$ layers with the interlayer spaces filled by the alkali metal atoms. The only exception is the manganese phase, for which a mixture of manganese and sodium atoms is observed in and between the layers. A projection view perpendicular to the layers provide more structural details (Fig. 5f-j). LiNa*M*[PO_4]F (*M* = Ni and Mg) contains infinite chains of edge-sharing octahedra (Fig. 5j), whereas $Na_2M[PO_4]F$ (*M* = Mn-Ni, and Mg) contain infinite chains of dimer units (face-sharing octahedra) sharing corners (Fig. 5f-i). Depending on the size of the transition metal, the dimer units point to different directions (Fig. 5k-n). In $Na_2M[PO_4]F$(*M* = Fe, Co, and Mg) all the dimer units point to the same direction (Fig. 5k), whereas in $Na_2M[PO_4]F$(*M* = Ni and Mn), we observe an alternation of two chains with the dimer units pointing to the right and two chains with the dimer units pointing to the left (Fig. 5l, m). The structural transition from edge- to face-sharing octahedra is mainly due to the tilting of a few PO_4 tetrahedra. Furthermore, since the tilted tetrahedra are different from phase to phase, this induces different orientations for the dimer units built of face-sharing octahedra (Fig. 5k-n). From a theoretical point of view, it would also be possible to build a theoretical structure in which one chain with the dimer units pointing to the right alternates with one chain with the dimer units pointing to the left (Fig. 5d, i, n). The predicted crystallographic data of this theoretical phase are given in Table 3.

Table 3. Crystallographic data of the $A_2M[PO_4]F$ theoretical structure ($P2_12_12$, Z = 4, *a* = 5.1991 Å, *b* = 11.6557 Å, *c* = 6.8489 Å, and *V* = 415.04 $Å^3$).

Atom	Wyck.	x	y	z
*A*1	4*c*	0.25367	0.83112	0.75500
*A*2	4*c*	0.24405	0.57990	0.49245
M	4*c*	0.78012	0.92680	0.97370
P	4*c*	0.29525	0.83807	0.23435
O1	4*c*	0.08875	0.64283	0.79617
O2	4*c*	0.65387	0.59587	0.92930
O3	4*c*	0.74525	0.79147	0.78667
O4	4*c*	0.71836	0.61910	0.56725
F1	2*a*	1/2	1/2	0.24880
F2	2*b*	0	1/2	0.18910

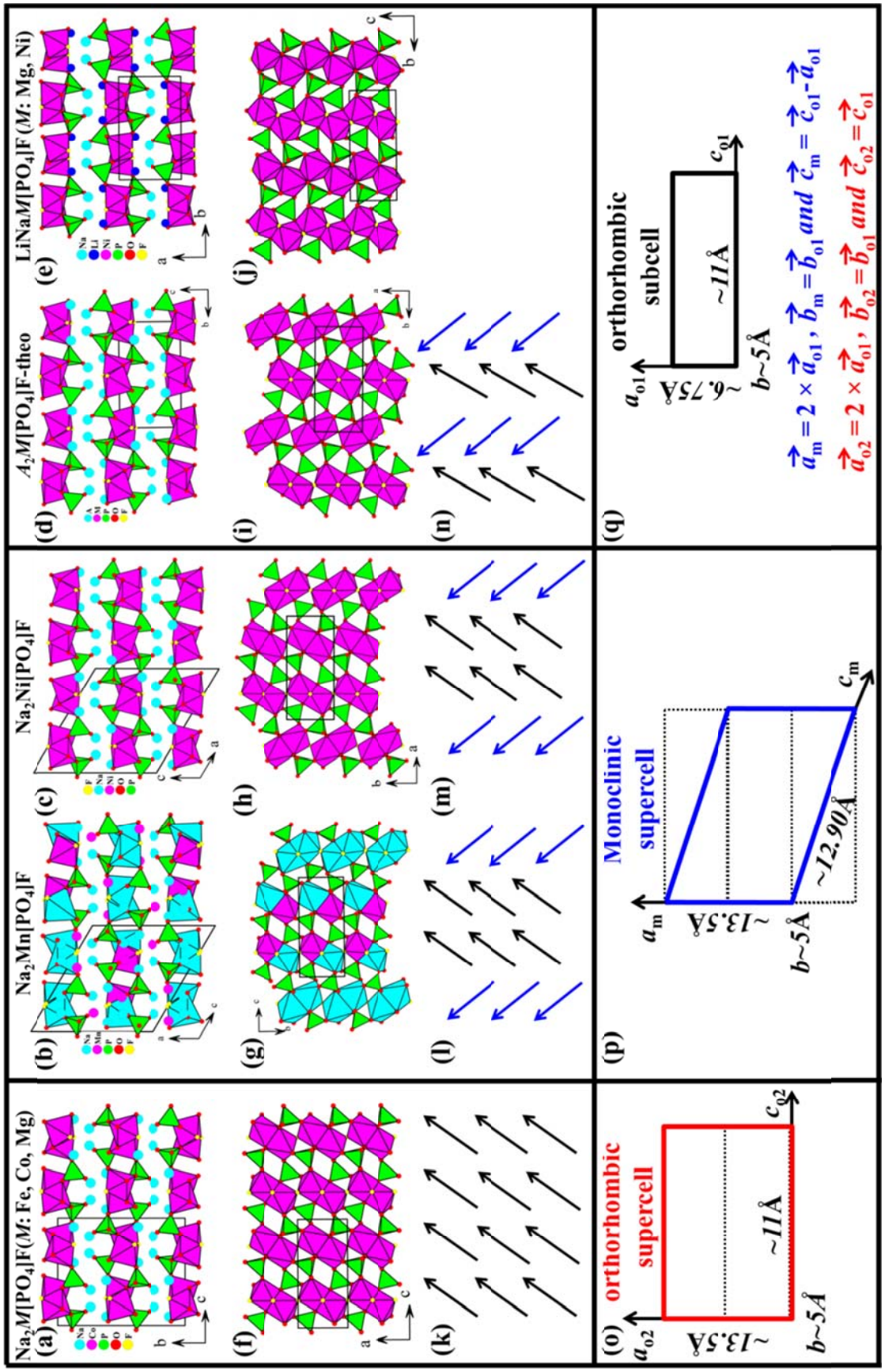

Fig. 5. Crystal structures of the $A_2M[PO_4]F$ compounds (A = Li and Na; M = Mn-Ni, and Mg).

3.4. Magnetic structure and properties of LiNaNi[PO_4]F

3.4.1. LiNaNi[PO_4]F magnetic properties

The results of magnetic susceptibility measurements for LiNaNi[PO_4]F are presented in Fig. 6. The magnetic susceptibility χ as a function of temperature revealed a signature of a magnetic transition at T ~ 5 K. Above ~ 170 K the corresponding χ^{-1} curve follows the Curie-Weiss law. A linear fit in the range 200-300 K yields Θ = -16.5 K and an effective moment 3.21 μ_B. The former indicates predominantly antiferromagnetic (AFM) interactions in the system and the latter is a typical value for S = 1 Ni^{2+}.[45] It is also noteworthy that despite the overall AFM nature of the magnetically ordered state below the transition temperature, the rise of the $\chi \cdot T$ product as a function of temperature on cooling below ~30 K suggests that the composition initially develops short-range ferromagnetic (FM) correlations until the long-range AFM structure sets in at T_N ~ 5 K. This behaviour is fully consistent with the bulk magnetic structure as determined from the neutron powder diffraction data and discussed below.

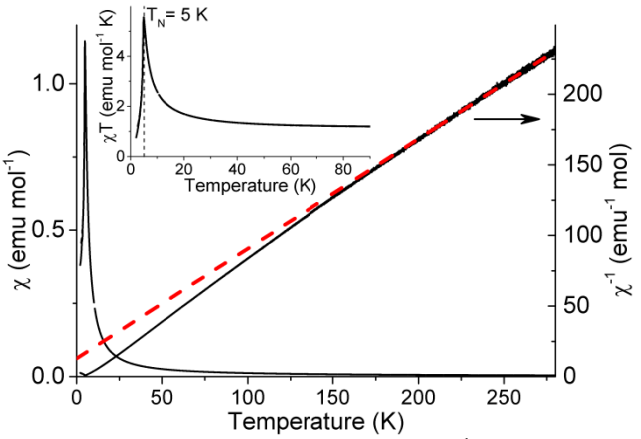

Fig. 6. Magnetic susceptibility χ, its inverse χ^{-1}, and χT product (inset) as a function of temperature for LiNaNi[PO_4]F. The red dashed line shows the linear fit with the Curie-Weiss function.

3.4.2. LiNaNi[PO_4]F magnetic structure from neutron powder diffraction data

Examination of the NPD patterns collected at 3 K and 6 K revealed additional diffraction peaks due to magnetic ordering (Fig. 7a).[46] This is consistent with the magnetic susceptibility data which suggested an AFM transition at ~ 5 K (Fig. 6). All the diffraction peaks of magnetic origin could be indexed by a unit cell doubled along a axis, i.e., with the propagation vector k = (1/2, 0, 0). For the 4e(x, y, z) Wyckoff site of the $P2_1/c$ space group, the magnetic representation decomposes in terms of four one-dimensional irreducible representations (IR) as $\Gamma = 3\Gamma_1 + 3\Gamma_2 + 3\Gamma_3 + 3\Gamma_4$. The associated basis vectors are listed in Table S8.† The best agreement between experimental and calculated NPD patterns was obtained for the Γ_1 (GxFyGz) representation (equivalent to the $P2_1'/c$ Shubnikov group, Opechowski-Guccione number 14.3.88). Furthermore, examination of the diffraction data showed no evidence of the scattering corresponding to magnetic moment components along the a or c axis, and therefore only the parameter defining the moment along b axis was refined. The Rietveld plot and crystallographic information are presented in Fig. 7b and Table S9,† respectively. The determined value of the moment, 1.87(4) μ_B, is close to that expected for d^8 Ni^{2+}. Assuming Brillouin function behaviour of the magnetization as a function of temperature, extrapolation to T = 0 for S = 1 and T_N = 5 K yields 2.12 μ_B as the ground state moment, similarly close to the theoretical value.

The magnetic structure of LiNaNi[PO_4]F arises due to an interesting combination of progressively weaker interactions along c, b, and a axes. The NiO_5F zigzag edge-sharing octahedral chains running along the c axis with the shortest Ni^{2+}-Ni^{2+} distances (~3.1Å) are ordered ferromagnetically by superexchange *via* common oxygen and fluorine atoms, as expected from the Goodenough-Kanamori rules.[47, 48]

The magnetic moments are perpendicular to the chain direction (Fig. 8), which is a typical case for (quasi-)isolated magnetic chains.[49] Super-superexchange *via* phosphate groups often results in AFM coupling; however, in the case of LiNaNi[PO_4]F one of the two Ni-O---O angles in each M-O---O-M interchain link appears to be severly bent to ~98° and as a result the chains are coupled ferromagnetically, forming FM quasi-layers in the b-c plane (Fig. 8a, b). Finally, the order between the layers is supported likely by a combination of exchange and dipole-dipole interactions which is consistent with the in-plane moment orientation in the FM quasi-layers favoured by the latter[49,50].

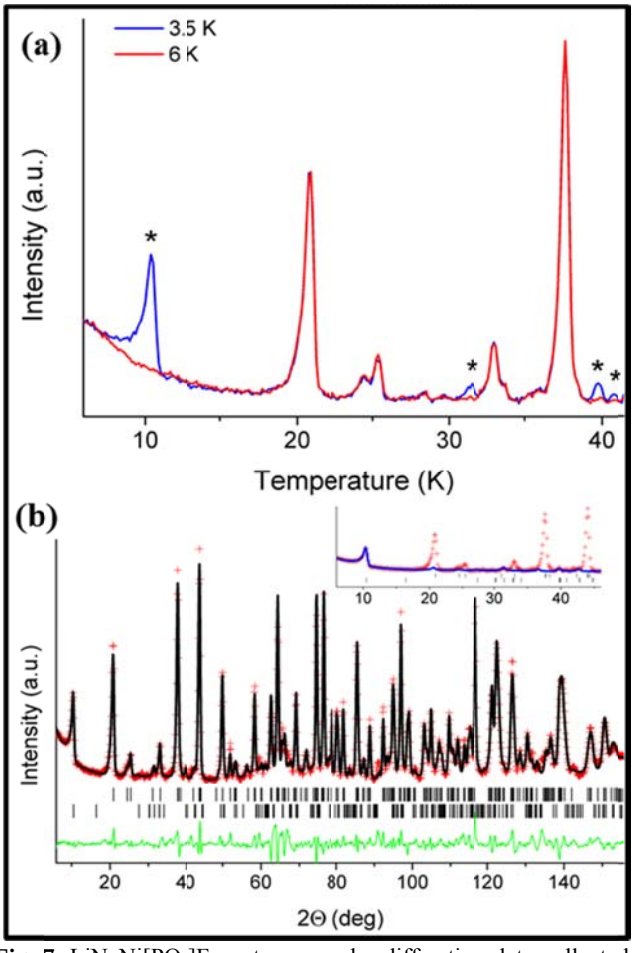

Fig. 7. LiNaNi[PO_4]F neutron powder diffraction data collected at 3 K and 6 K. Additional peaks observed at low temperature are indicated with asterisk symbols (a). Rietveld plot for the LiNaNi[PO_4]F neutron powder diffraction data collected at 3 K

(b). The red crosses and black and green solid lines indicate the observed and calculated patterns and their difference, respectively. The tick marks indicate the position of the diffraction peaks. R_p = 4.89%, R_{wp} = 6.68%, R_F = 2.99%, R_{mag} = 10.6%.[46] The blue curve in the inset shows magnetic contribution.

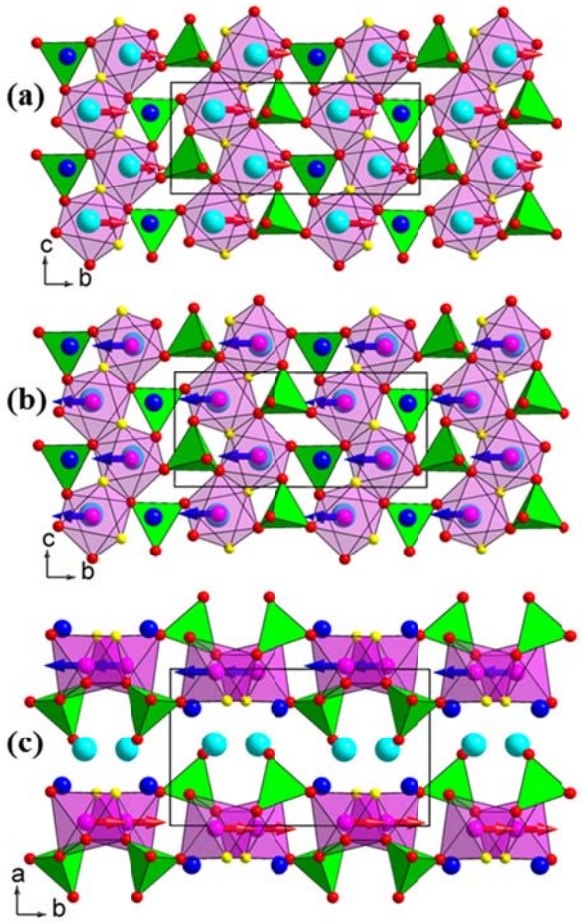

Fig. 8. Views of the ferromagnetically ordered Ni[PO_4]F layers at x = 0 (a), and x = 1 (b) and view of the magnetic structure of LiNaNi[PO_4]F with antiferromagnetic coupling between the layers (c).

4. Conclusions

The crystal structure study of the $Li_{2-x}Na_xMg[PO_4]F$ system ($0 \leq x \leq 2$) led to the discovery of two new compounds $Li_2Mg[PO_4]F$ and LiNaMg[PO_4]F. These phases are isostructural to $Li_2Ni[PO_4]F$ and LiNaNi[PO_4]F, respectively. The inspection of the different crystallographic databases revealed strong relationships among the fluorophosphates $A_2M[PO_4]F$ (A = Li and Na; M = Mn-Ni, and Mg) and oxides such as β-Nb[PO_4]O and $Ca_3[SiO_4]O$. More interestingly, the group-subgroup transformation schemes showed that all the $Na_2M[PO_4]F$ (M = Mn-Ni, and Mg) phases can be described as layered structures. The main difference between these compounds is the different orientations of the PO_4 tetrahedra plus, in some cases ($Na_2Mn[PO_4]F$), a permutation between the alkali- and the transition-metal atoms. This difference is mainly related to the size of the transition-metal and alkali-metal atoms. The magnetic structure of LiNaNi[PO_4]F as determined from NPD data can be described as AFM coupling of FM quasi-layers of zigzag edge sharing octahedral chains, in turn connected to each other *via* phosphate groups. The magnetic moment is perpendicular to the chain direction and is close to the theoretical value for d^8 Ni^{2+}.

Acknowledgments

This work was financially supported by the Japan Society for the Promotion of Science (JSPS) Fellows Grant Number 24•02506. CDL received support for this work from the Australian Research Council – Discovery Projects (DP110102662).

References

1 H. Ben Yahia, *Ph.D. thesis,* Bordeaux University, France, 2006.
2 A. K. Pahdi, K. S. Nanjundaswamy, J. B. Goodenough, *J. Electrochem.Soc.* 1997, **144**, 1188-1194.
3 K. Zaghib, A. Guerfi, P. Hovington, A. Vijh, M. Trudeau, A. Mauger, J.B. Goodenough, C.M. Julien, *J. Power Sources* 2013, **232**, 357-369.
4 R Malik, A Abdellahi, G. Ceder, *J. Electrochem. Society* 2013, **160 (5)**, A3179-A3197.
5 Y Zhang, Q.-Y. Huo, P.-P. Du, L.-Z. Wang, A.-Q. Zhang, H. Y.- Song, Y. Lv, G.-Y. Li, *Synthetic Metals* 2012, **162**, 1315–1326.
6 E. Gaudin, H. Ben Yahia, J. Darriet, *Phosphorus Research Bulletin* 2005, **19**, 19-24.
7 S. Okada, M. Ueno, Y. Uebou, J. I. Yamaki, *J. Power Sources* 2005, **146**, 565-569.
8 M. Nagahama, N. Hasegawa, S. Okada, *J. Electrochem. Soc.* 2010, **157 (6)**, A748-A752.
9 S.-W. Kim, D.-H. Seo, H. Kim, K.-Y. Park, K. Kang, *Phys. Chem. Chem. Phys.* 2012, **14**,3299-3303.
10 T. N. Ramesh, K. T. Lee, B. L. Ellis, L. F. Nazar, *Electrochem. Solid-State Lett.* 2010, **134**, A43-A47.
11 N. Recham, J. N. Chotard, J. C. Jumas, L. Laffont, M. Armand, , J.M. Tarascon, *Chem. Mater.* 2010, **22**, 1142-1148.
12 H. Ben Yahia, M. Shikano, K. Tatsumi, S. Koike, H. Kobayashi, *Dalton trans.* 2012, **41**, 5838-5847.
13 H. Ben Yahia, M. Shikano, S. Koike, K. Tatsumi, H. Kobayashi, H. Kawaji, M. Avdeev, W. Miiller, C.D. Ling, J. Liu, M.-H. Whangbo, *Inorg. Chem.* 2012, **51**, 8729-8738.
14 H. Ben Yahia, M. Shikano, H. Sakaebe, S. Koike, M. Tabuchi, H. Kobayashi, H. Kawaji, M. Avdeev, W. Miiller, C.D. Ling, *Dalton trans.* 2012, **41**,11692-11699.
15 H. Ben Yahia, M. Shikano, S. Koike, H. Sakaebe, M. Tabuchi, H. Kobayashi, *J. Power Sources* 2013, 10.1016/j.jpowsour.2013.03.128.
16 H. Ben Yahia, M. Shikano, H. Sakaebe, H. Kobayashi, *Mater. Chem. Phys.* 2013, **141**, 52-57.
17 H. Ben Yahia, M. Shikano, H. Kobayashi, to be submitted.
18 V. Petricek, M. Dusek, L. Palatinus, Jana2006. The crystallographic computing system. Institute of Physics, Praha, Czech Republic 2006.
19 M.C. Burla, M. Camalli, B. Carrozzini, G. Cascarano, C. Giacovazzo, G. Polidori, R. Spagna, *J. Appl. Crystallogr.* 2003, **36**, 1103.
20 A. L. Spek, 2008 PLATON, A Multipurpose Crystallographic Tool, Utrecht University, Utrecht, The Netherlands.
21 I. D. Brown, D. Altermatt, *Acta Crystallogr. B* 1985, **41**, 244-247.
22 N. E. Brese, M. O'Keefe, *Acta Crystallogr. B* 1991, **47**, 192-197.
23 S.H. Swafford, E.M. Holt, *Solid State Sci.* 2002, **4**, 807-812.
24 R.D. Shannon, *Acta Crystallogr., Sect. A: Cryst. Phys., Diffr., Theor. Gen. Crystallogr.* 1976, **32**, 751-767.
25 O. Andac, F. P. Glasser, R. A. Howie, *Acta Crystallogr. C: Cryst. Struct. Commun.* 1997, **53**, 831-833.
26 M. Perez Mendez, R. A. Howie, F. P. Glasser, *Cem. Concr. Res.* 1984, **14**, 57-63.
27 H. Bärnighausen, *Commun. Math. Chem.* 1980, **9**, 139-175.
28 H. Bärnighausen, U. Müller, Symmetriebeziehungen zwischen den Raumgruppen als Hilfsmittel zur straffen Darstellung von Strukturzusammenhängen in der Kristallchemie, University of Karlsruhe and University/GH Kassel, Germany, 1996.
29 F. Sanz, C. Parada, C. R. Valero, *J. Mater. Chem.* 2001, **11**, 208-211.

30 O.V. Yakubovich, O.V. Karimova, O.K. Mel'nikov, *Acta Crystallogr. C* 1997, **53**, 395.
31 Y.K. Kabalov, M.A. Simonov, N.V. Belov, *Dokl. Akad. Nauk SSSR.* 1974, **215**, 850-853.
32 B. L. Ellis, W. R. M. Makahnouk, W. N. R. Weetaluktuk, D. H. Ryan, L. F. Nazar, *Chem. Mater.* 2010, **22**, 1059-1070.
33 N.A. Nosyrev, E.N. Treushnikov, V.V. Ilyukhin, N.V. Belov, *Dokl. Akad. Nauk SSSR* 1974, **216**, 82-85.
34 E.N. Treushnikov, V.V. Ilyukhin, N.V. Belov, *Dokl. Akad. Nauk SSSR* 1970, **190**, 334-337.
35 A. LeClaire, H. Chahboun, D. Groult, B. Raveau, *Z. Kristallogr*. 1986, **177**, 277-286.
36 D. L. Serra, S.-J. Hwu, *Acta Crystallogr*. *C* 1992, **48**, 733-735.
37 U. Kaiser, G. Schmidt, R. Glaum, R. Gruehn, *Z. Anorg. Allg. Chem.* 1992, **607**, 113-120.
38 N.G. Chernorukov, N.P. Egorov, E.V. Shitova, Y.I. Chigirinskii, *Russ. J. Inorg. Chem.* 1981, **26**, 1454-1456.
39 J.M. Amarilla, B. Casal, E. Ruiz Hitzky, *J. Mater. Chem.* 1996, **6**, 1005-1011.
40 M.A.K. Ahmed, H. Fjellvag, A. Kjekshus, *J. Inorg. Nucl. Chem.* 1977, **39**, 1239-1240.
41 S.L. Wang, C.C. Wang , K.H. Lii, *J. Solid State Chem.* 1989, **82**, 298-302.
42 L.F. Schneemeyer, L. Guterman, T. Siegrist, G.R. Kowach, *J. Solid State Chem.* 2001, **160**, 33-38.
43 T.A. Zhadanova, L.N. Demianets, A.A. Voronkov, Y.A. Piatenko, *Dokl. Akad. Nauk SSSR* 1975, **224**, 1069-1072.
44 H. Krüger, V. Kahlenberg, *Z. Kristallogr.* 2008, **223**, 382–388.
45 R. L. Carlin, 1986. Magnetochemistry. Berlin et al.: Springer.
46 J. Rodriguez-Carvajal, *Phys. B* 1993, **192**, 55-69.
47 J. B. Goodenough, Magnetism and the chemical bond. Interscience Publishers New York: 1963; Vol. 1.
48 J. Kanamori, *J. Phys. Chem. Solids* 1959, **10**, 87-98.
49 L. J. De Jongh, A. R. Miedema, *Advances in Physics* 1974, **23**, 1-260.
50 P. Bruno, *Phys. Rev. B* 1991, **43**, 6015-6021.

Dalton Transactions

Dalton Transactions

Dynamic Article Links ►

Cite this: DOI: 10.1039/c0xx00000x

www.rsc.org/materials

Synopsis

Structural relationships among LiNaMg[PO_4]F and Na_2M[PO_4]F (M = Mn-Ni, and Mg), and the magnetic structure of LiNaNi[PO_4]F

Hamdi Ben Yahia[a,*], Masahiro Shikano[a,*], Hironori Kobayashi[a], Maxim Avdeev[b], Samuel Liu[c], Chris D. Ling[c]

Received (in XXX, XXX) Xth XXXXXXXXX 2011, Accepted Xth XXXXXXXXX 20XX

DOI: 10.1039/b000000x

Synopsis